Single-Particle Ratiometric Pressure Sensing Based on “Double-Sensor” Colloidal Nanocrystals

Monica Lorenzon†Orcid, Valerio Pinchetti†, Francesco Bruni†, Wan Ki Bae‡Orcid, Francesco Meinardi†, Victor I. Klimov*‡Orcid, and Sergio Brovelli*†Orcid

Abstract

Ratiometric pressure sensitive paints (r-PSPs) are all-optical probes for monitoring oxygen flows in the vicinity of complex or miniaturized surfaces. They typically consist of a porous binder embedding mixtures of a reference and a sensor chromophore exhibiting oxygen-insensitive and oxygen-responsive luminescence, respectively. Here, we demonstrate the first example of an r-PSP based on a single two-color emitter that removes limitations of r-PSPs based on chromophore mixtures such as different temperature dependencies of the two chromophores, cross-readout between the reference and sensor signals and phase segregation. In our approach, we utilize a novel “double-sensor” r-PSP that features two spectrally separated emission bands with opposite responses to the O2 pressure, which boosts the sensitivity with respect to traditional reference-sensor pairs. Specifically, we use two-color-emitting dot-in-bulk CdSe/CdS core/shell nanocrystals, exhibiting red and green emission bands from their core and shell states, whose intensities are respectively enhanced and quenched in response to the increased oxygen partial pressure that effectively tunes the position of the nanocrystal’s Fermi energy. This leads to a strong and reversible ratiometric response at the single particle level and an over 100% enhancement in the pressure sensitivity. Our proof-of-concept r-PSPs further exhibit suppressed cross-readout thanks to zero spectral overlap between the core and shell luminescence bands and a temperature-independent ratiometric response between 0 and 70 °C.

KEYWORDS:Ratiometric oxygen sensing pressure sensitive paints dot-in-bulk nanocrystals core/shell dual color emission photocharging

Pressure sensitive paints (PSPs) are effective, nonintrusive tools capable of mapping gas flows near complex surfaces and reporting on the concentration of oxygen in gas mixtures through remote optical detection. The foremost use of PSPs is in aerospace engineering with applications ranging from aerodynamic tests of aircraft prototypes (1, 2) to fundamental studies in acoustics, (3) shock-wave propagation, and transonic buffeting effects (4) (see Figure 1a,b). PSPs are also widely used in the design of complex fluidic and microfluidic systems, (5) including supersonic micronozzles, (6) microfluidic oscillators, (5) microchannels, (7) and in studies of pressure, heat-transfer, and shear stress in micromechanical devices (8) (Figure 1a,b). Furthermore, PSPs are employed in environmental monitoring, (9) marine research, (10) the food packaging industry, (11) medicine, (12) and biology, (13) and are particularly effective to detect a few orders of magnitude of pressure variations. Traditional PSPs consist of an oxygen sensitive organic chromophore dispersed in a porous organic (14) or inorganic (3, 15) matrix (commonly referred to as a “binder”). When exposed to O2, the luminescence of the chromophore is quenched proportionally to the oxygen partial pressure, thus allowing for real-time pressure monitoring. (16-18) The all-optical working mechanism of PSPs makes these devices substantially simpler than conventional piezoresistive (19) or MEMS-based transducers (20) that require the integration of the sensors and the wiring on the investigated surfaces, which hinders their applications in the case of moving or miniaturized parts. (20) In addition, traditional nonoptical sensors yield pointlike pressure measurements, while PSPs allow one to map the gas flow with high spatial resolution on extended or complex surfaces with a single optical scan. (3, 21) This largely simplifies data collection and processing, which is particularly challenging in the case of turbulent or supersonic gas flows. (22)

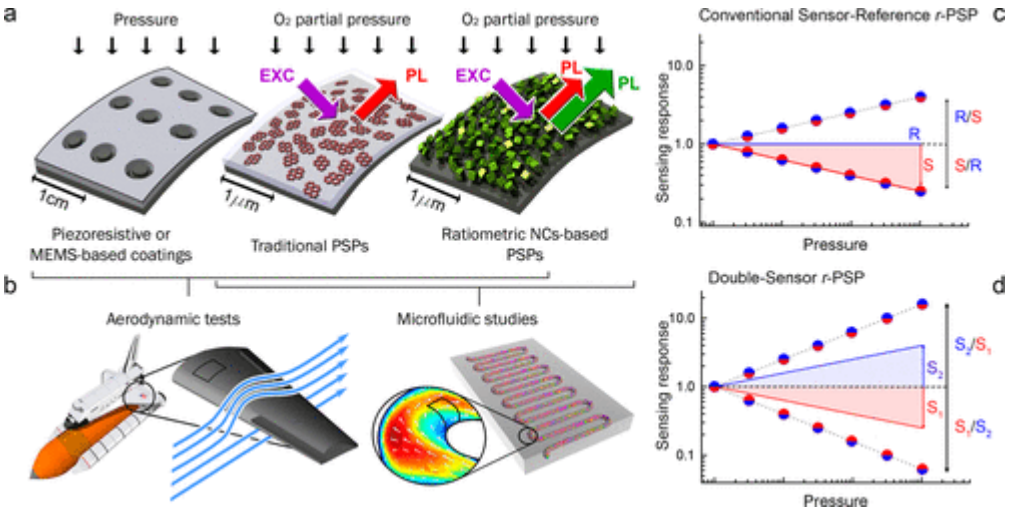

Figure 1. Working principles of single- and double-sensor ratiometric PSPs. (a) Illustration of different technologies for pressure measurements: (left) traditional MEMS-based transducers, (center) traditional organic chromophore-based PSPs, and (right) DiB NC-based ratiometric PSPs. (b) All of the pressure sensors from panel a can be used in (left) aerodynamic tests on model surfaces, whereas (right) microfluidic systems can be investigated only by means of PSPs. Representative plots of the ratiometric response of (c) conventional r-PSPs featuring an inert (pressure-insensitive) reference (R, blue line) and an O2 sensitive emitter (S, red line). The ratiometric response (circles) is determined by the sensitivity of the sensor only (S/R or R/S ratio shown as red/blue circles and blue/red circles respectively). (d) Ratiometric response of a double-sensor r-PSPs consisting of two O2 sensing emitters (S1 and S2) with opposite luminescence responses. In this case, the ratiometric response (circles) can be expressed as S1/S2 or S2/S1; in either case, it is strongly amplified with respect to the sensitivity of the individual sensor species.

State-of-the-art organic PSP chromophores, such as metal porphyrins, (23) pyrenes, (24) and Ru(II) or Pt(II) complexes, (25) have good oxygen sensitivity but suffer from limited thermal (26) and photochemical (27) stability. The interaction with O2, which generates singlet oxygen radicals, accelerates photodegradation under UV illumination, (21, 22) leading to luminescence drops ranging from 1%/hour (refs 1 and 21) up to 15%/hour (ref 28). In addition, the temperature dependence of the luminescence efficiency, typical of organic chromophores, introduces bias errors to the pressure data collected on different model parts and therefore requires continuous monitoring of the surface temperature and specific calibration protocols. (1, 3, 4, 29) Mixtures of O2-sensitive and temperature-sensitive chromophores, operating as pressure and temperature references for the other emitter, have been proposed to address this problem. (30, 31) These PSPs require, however, effective encapsulation of the temperature sensor in oxygen-impermeable polymers to avoid cross-sensitivity issues. (3, 32)

Colloidal semiconductor nanocrystals (NCs) have been recently proposed as potentially alternative sensing materials. (33-41) NCs combine high-emission efficiency (42-44) and size-tunable electronic properties (45, 46) with enhanced stability and exceptionally large surface-to-volume ratios. (36, 47) Similarly to organic chromophores, O2 sensing with NCs relies on quenching of the luminescence intensity under O2 flow, mostly due to ultrafast extraction of surface and photogenerated electrons by oxygen. (48) From the physical perspective, the extraction of electrons from the NCs by exposing them to O2 replicates the effect of lowering the Fermi level by applying a positive (oxidative) potential in electrochemical measurements. In direct analogy, the removal of oxygen from the NC surroundings resembles the effect of raising the Fermi level under negative (reducing) electrochemical potentials. (49-51) An advantageous feature of NCs from the standpoint of potential PSP applications is that the coupling of photogenerated carriers with phonons in these systems is much weaker than in organic chromophores, (52) which results in a smaller variation of

the emission quantum yield in the temperature range typically explored in PSP studies (10–40 °C). (3, 4, 29, 31) Reported examples of O2-responsive NCs include CdSe, (38) CdTe, (39) and CdSe/ZnS core/shell systems. (53) These structures have been utilized for humidity detection and dry gas sensing, as well as biological sensing applications. (54) As distinct from organic chromophores, the use of NCs as PSPs emitters potentially eliminates the need for the binder, as NCs can be deposited directly onto tested surfaces (Figure 1a). This is particularly advantageous for high-frequency sensing (4) because the rate-determining process in the sensing response is typically the permeation of a gas into the binder, (1) which protracts the response time from a few microseconds with porous matrices (4) to tens of seconds for traditional polymeric binders. (55)

A common experimental difficulty of radiometric luminescence mapping using organic chromophores or conventional NC-based PSPs is that they require accurate quantitative measurements of the emission intensity across extended or complex surfaces under oxygen flow and UV irradiation. For this reason, wind tunnel aerodynamic tests are typically performed by comparing the results of “wind-on” and “wind-off” measurements in order to account for the experimental geometry, model misplacements, (1, 22, 48) nonuniform distribution of the chromophore in the binder and an uneven thickness of the binder layer across the model surface. (22, 29, 56)

Some of these issues have been addressed through the use of so-called ratiometric PSPs (r-PSP) that exploit the different sensitivity to O2 of two (or more) chromophores to detect and quantify local pressure variations. A conventional r-PSP consists of an O2-insensitive chromophore (the “reference”) acting as an internal standard for the luminescence intensity of an O2-responsive emitter (the “sensor”), as depicted in Figure 1c. Examples of reported two-component r-PSPs include mixtures of organic dyes (22) and dye–polymer conjugates (57) as well as organic/inorganic hybrid systems such as binary blends of dyes and NCs, (15, 22) NC-polymer nanocomposites, (15, 58) and dye-functionalized NCs. (33) Although these systems remove the need for the wind-off/wind-on calibration, their use is still associated with several experimental difficulties arising from (i) the different temperature dependences of the two chromophores, (22, 59) (ii) cross-readout errors due to the spectral overlap between the emission bands of the reference and the sensor (60) species, and (iii) spatial inaccuracy due to inhomogeneous distribution of the emitters on the model surfaces or in the binder, (60) whose effects are aggravated by intermolecular interactions leading to exciton migration processes. (48, 57)

Here we demonstrate that all of these limitations can be alleviated using r-PSPs based on a single dual-color emitter that features intrinsic ratiometric response at the single particle level, suppressed cross-readout due to a vanishing overlap between the luminescence spectra of the two emissive states, a dynamic range of ratiometric O2-pressure sensing of 3 orders of magnitude, and a virtually temperature-independent ratiometric response between 0 and 70 °C. An important advantage of our new approach is that it is based not on an inert (pressure-insensitive) reference, but instead combines two pressure-sensitive states in a single emitter and that these states exhibit opposite luminescence responses to changes in the oxygen pressure. In these “double-sensor” systems, one emission channel is quenched, while the other is concomitantly enhanced by the presence of O2, similarly to the so-called “reverse sensing” behavior recently found in CdSe colloidal quantum wells. (36)Figure 1c,d schematically compares the luminescence-versus-pressure dependence of a conventional reference–sensor pair (R and S, respectively) and that of a double-sensor (S1 and S2) r-PSP. Importantly, while the response of a conventional r-PSP featuring an inert reference is given solely by the sensor that determines the maximum ratiometric O2-sensitivity of the blend (either S/R or R/S in Figure 1c), replacing the inert reference with a “reverse” O2 sensor exhibiting enhanced luminescence when exposed to O2 (S2 in Figure 1d) leads to strongly amplified ratiometric sensitivity. We note that in the presence of two sensing species, the ratiometric response can be conveniently chosen (S1/S2 versus S2/S1) in order to better suit the experimental conditions, while ensuring in both cases enhanced sensitivity with respect to the conventional reference/sensor system.

Our “double-sensor”, single-emitter r-PSP uses CdSe/CdS dot-in-bulk (DiB) NCs that consist of a small CdSe core overcoated with an ultrathick CdS shell. (49, 61) Owing to their peculiar internal structure, DiB NCs are capable of simultaneously sustaining core and shell excitons, whose radiative recombination leads to two-color (red and green) luminescence under both low-intensity continuous wave (cw) optical excitation (61) and electrical injection. (49) Two essential structural features of these NCs are an abrupt core/shell confinement potential and an engineered interlayer of zincblende CdS separating the zincblende CdSe core from the thick wurtzite CdS shell. This peculiar structure of the core–shell interface slows down relaxation of shell-localized holes into core states, which leads to the development of efficient shell emission observed simultaneously with emission from the core. (62) Importantly for r-PSP applications, the shell excitons are exposed to the NC’s surface, and their luminescence is highly sensitive to nonradiative electron transfer to surface defects or molecular acceptors (in our case oxygen) adsorbed onto the NC surface, which leads to luminescence quenching. (63-65) In stark contrast, the emission arising from core-localized excitons is enhanced by exposure to O2 as the removal of extra electrons generated by photocharging helps quench nonradiative Auger recombination. (63) As a result of these effects, the two emission channels of the DiB NCs follow opposite trends with increasing/decreasing O2 partial pressure, which allows us to realize the double-sensor ratiometric response using a single emitter.

Results and Discussion

Optical Properties and Temperature Sensitivity of DiB NCs

The CdSe/CdS DiB NCs used in this study have been synthesized following the procedure reported in ref 49. Representative TEM images of the NCs and a statistical analysis of their dimensions are reported in Figure.S1. A representative optical absorption and photoluminescence (PL) spectra of the DiB NCs with core radius R = 1.5 nm and shell thickness H = 8.5 nm under cw excitation at 400 nm are reported in Figure 2a. The absorption spectrum shows a steep edge at ∼500 nm due to absorption by the thick CdS shell whose volume is ∼300 times larger than that of the CdS core. The PL spectrum consists of two well-separated emission peaks located at 632 and 512 nm. The 632 nm band is due to recombination of core excitons characterized by the decay rate RC = 5.5 × 106 s–1 (see Figure.S2a). The 512 nm peak arises from radiative decay of shell excitons which has the rate RS = 5 × 109 s–1 (Figure.S2b). As was established previously, (61) electrostatic repulsion between the core- and shell-localized holes leads to a dynamic Coulomb blockade of the core states; as a result, the intensity of the shell PL exhibits complex dependence on excitation fluence (Figure.S3). On the other hand, the core PL shows a more common pump-intensity dependence; it first grows linearly with pump power and then saturates at high NC occupancies. The details of pump-power dependence of core and shell PL bands, however, are inconsequential from the standpoint of ratiometric sensing, as pressure measurements usually utilize low-intensity excitation. As illustrated in Figure.S3 (highlighted in gray), in this case both emission bands scale linearly with excitation fluence for the pump-intensity change by more than 2 orders of magnitude. Microscale pressure studies are affected by the exact type of PL pump-intensity-dependence to an even lesser degree, as they are typically performed at fixed excitation powers using focused light with a spot area comparable to the sample size. Most importantly for ratiometric sensing, both the core and the shell emission intensities (IC, IS) show nearly identical trends across a wide range of temperatures (0–70 °C), which covers a typical range of temperature variation for many PSPs applications (10–50 °C, refs 3 and 31). This results in the remarkable temperature stability of the ratiometric response of DiB NCs, which, in Figure 2b, is evaluated in terms of the variation of the IC/IS ratio as a function of temperature. The same figure also shows the relative first derivative of the luminescence ratio, (d(IC/IS)/dT)/(IC/IS), which emphasizes the absence of variations or drops in the ratiometric response over the whole range of investigated temperatures.

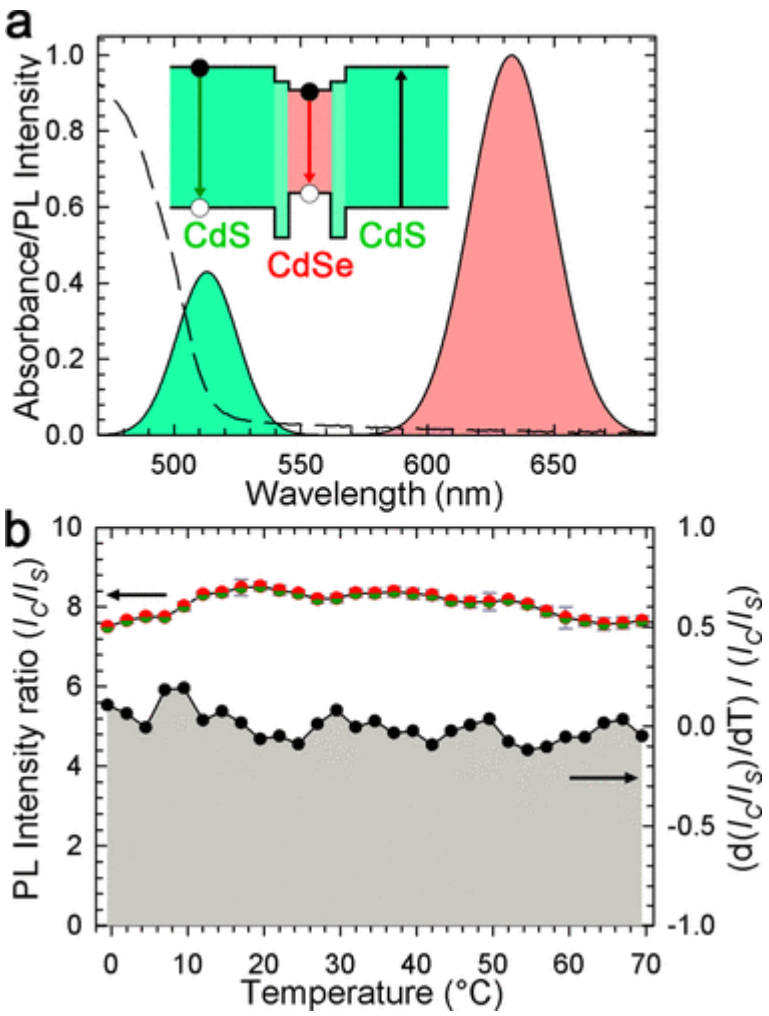

Figure 2. Optical properties and temperature sensitivity of DiB NCs. (a) Optical absorption (dashed line) and normalized photoluminescence spectrum of a hexane solution of CdSe/CdS DiB NCs with the 1.5 nm core radius and the 8.5 nm shell thickness. Core and shell emission bands are highlighted by red and green shadings, respectively. Inset: An approximate band diagram of CdSe/CdS DiB NCs, featuring an interfacial zincblende CdS layer that separates a zincblende CdSe core from a wurtzite CdS shell. (b) Temperature dependence of the ratio of the core and the shell spectrally integrated PL intensities (IC/IS, red/green symbols) and the relative first derivative of the (IC/IS) ratio versus T dependence. All measurements were performed using the 15 μJ/cm2 excitation fluence and the excitation wavelength of 400 nm.

We can quantify the temperature sensitivity (ST) of the DiB NCs through the expression ST = −[IC(T2)/IS(T2) – IC(T1)/IS(T1)]/(T2 – T1), where IC,S(T1) and IC,S(T2) are the intensities of the core and shell emission measured at the two extremes of the temperature range. (1) By considering the temperature range from T1 = 0 °C to T2 = 70 °C, we obtain the remarkably low value of ST of only 0.01%/°C; this is significantly lower than that for the state-of-the-art two-component r-PSPs, which exhibit ST of 0.05–1.5%/°C. (1) We note, however, that the temperature trend of IC/IS is not monotonic, as commonly observed for traditional r-PSPs, (22) but shows a slight increase from 0 to 20 °C, followed by a small drop with increasing temperature. In order to account for this trend, we have derived the maximum temperature sensitivity, STM, as the maximum variation of (d(IC/IS)/dT)/(IC/IS), which could also arise from slight fluctuations of the position of the excitation spot during the measurements due to sample misplacement in the cryostat. Using this approach, we obtain STM = 0.19% around 10 °C, which is still comparable to state-of-the-art PSPs.

Ratiometric Oxygen Sensing Using DiB NCs

We proceed with demonstrating the ratiometric O2 sensing ability of DiB NCs by monitoring the evolution of their PL spectrum during stepwise pressure ramps from P = 1 to 10–3 bar. In these experiments, a submonolayer film of DiB NCs with core radius R = 1.5 nm and shell thickness H = 8.5 nm is dip-casted onto a glass substrate, which allows for homogeneous coverage of the surface as shown in Figure.S4. The luminescence of the sample is excited by 400 nm light and continuously collected with a CCD camera, while the sample chamber (originally filled with O2) is progressively evacuated through rapid pressure steps. For each step, the pressure is lowered by a factor of 10 and maintained constant for 90 s. After the final step at 10–3 bar, the chamber was refilled stepwise with O2 following the same procedure. Because the O2 concentration is proportional to the total pressure, these measurements directly yield ratiometric estimations of the pressure on the sample surface similarly to what is typically achieved with PSPs. As evident from the PL spectra in Figure 3a, the core and shell PL intensities demonstrate the opposite trends in response to changes in the chamber pressure. Specifically, the core PL undergoes progressive dimming upon evacuation, while the shell emission increases and becomes dominant at P = 10–3 bar. Importantly, refilling the sample chamber with nitrogen does not lead to recovery of the PL intensity, which confirms the essential role of oxygen in the sensing response.

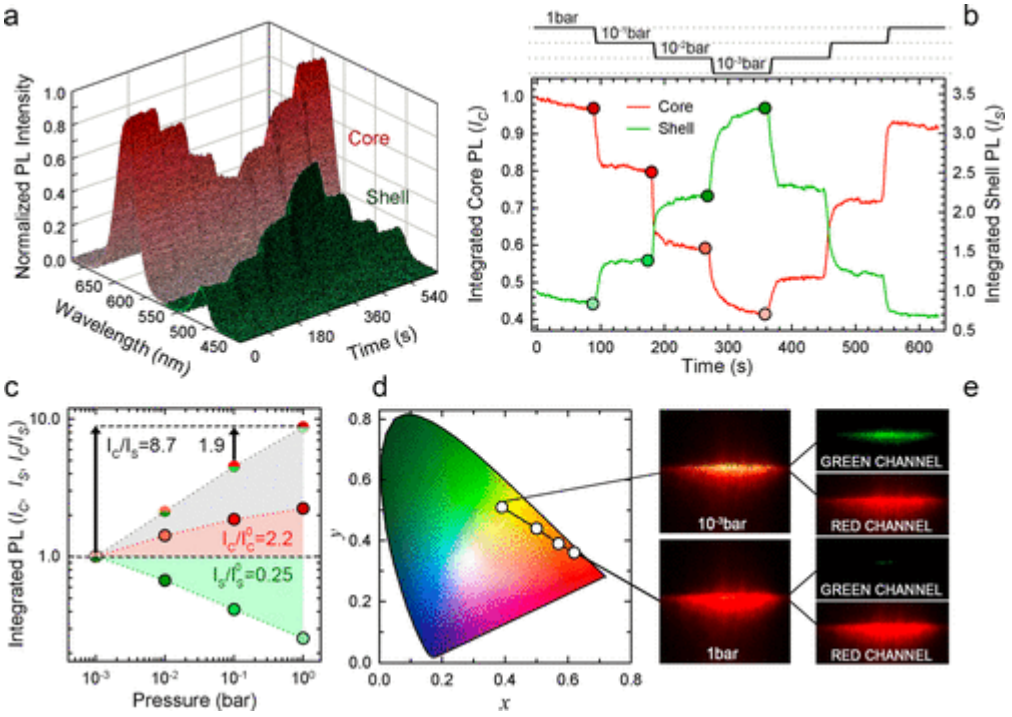

Figure 3. Ratiometric oxygen sensing experiments with DiB NCs. (a) A series of PL spectra (1 s acquisition time per frame, 90 s steps) during a stepwise pressure scan. The pressure is reduced rapidly and kept constant for 90 s, starting from atmospheric pressure (P = 1 bar) to 10–1, 10–2, and 10–3 bar, after which the sample chamber is stepwise refilled up to the initial pressure level of P = 1 bar. (b) Integrated PL intensities of the core (IC, red line) and the shell (IS, green line) extracted from the stepwise pressure scan in panel a. Both trends are normalized to the initial PL intensity at P = 1 bar. (c) The IC and IS values (red and green dots, respectively) and the IC/IS ratio (red/green dots) as a function of increasing pressure (logarithmic scale). All trends are normalized to their respective value at P = 10–3 bar (I0C and I0S respectively). All measurements were performed using the 5 μJ/cm2 excitation fluence and the excitation wavelength of 400 nm. (d) Overall emission color of a DiB NC film extracted from the PL spectra in panel a and projected onto the CIE chromaticity diagram. (e) Photographs of a DiB NCs sample at oxygen pressure

of 1 bar and 10–3 bar (bottom left and top left, respectively) under UV illumination collected using UV-filtered camera (illumination spot 1 cm × 1 cm, excitation power density ∼50 mW/mm2). The signals detected selectively by the red and green channels are reported in the right panels for direct confirmation of suppressed cross-readout.

The observed difference between the O2 response of the core and the shell PL can be rationalized by considering the electron withdrawing nature of molecular oxygen, which in the ground state is a diradical triplet with strong electron-accepting character. As a result, O2 is capable of efficiently extracting electrons from both the quantized states (66) of the NCs and electron-rich surface defects that thereby become capable of trapping photogenerated electrons from the NC conduction band. (36) Similarly to the effect of raising the NC Fermi level obtained by either applying a negative electrochemical potential or direct electric bias in light-emitting diodes, (49, 63) the removal of oxygen progressively suppresses electron trapping, leading to the observed strong enhancement of the green luminescence due to increased radiative recombination efficiency of shell excitons. On the other hand, as observed previously (67, 68) and confirmed by our time-resolved PL measurements in controlled atmosphere (see a detailed discussion later in this work), the dimming of the core PL is associated with nonradiative Auger recombination of negatively charged core excitons (negative trions), which are formed due to accumulation of excess electrons in the NCs in the absence of electron withdrawing O2 molecules. A similar effect has previously been observed with other CdSe/CdS heterostructures including thick-shell NCs (67, 68) and colloidal nanoplatelets. (36)

In order to quantify the ratiometric luminescence response of DiB NCs, in Figure 3b we report the spectrally integrated core and shell PL intensities extracted from Figure 3a, both normalized to their initial values at P = 1 bar. Each steplike variation of the O2 pressure leads to a concomitant modulation of both emission bands. Specifically, lowering the pressure from 1 to 10–3 bar results in ∼60% dimming of IC and over 300% increase of IS. Upon ramping the O2 pressure back up to 1 bar, both the core and the shell emission bands fully recover their original intensities. The opposite sign of the luminescence response of the core and the shell is emphasized in Figure 3c, where we report IC and IS collected at the end of each pressure step (highlighted with dots in Figure 3b) as a function of the O2 pressure. Thanks to this peculiar feature of DiB NCs, the ratiometric response considerably exceeds the sensing response of the individual emitting states with the enhancement reaching 100% with respect to IS and over 400% with respect to IC across the whole investigated pressure range. The ratiometric sensing response of our unoptimized DiB NCs between 1 and 0.1 bar is ∼1.9, which is comparable to that of commercial single-band (radiometric) and ratiometric PSPs, whose responses range between ∼2 and ∼4 (ref 69).

In order to evaluate the precision of the pressure measurement achievable with our NCs, we calculated the standard deviation of IC/IS in the last 50 s of each pressure step during refilling, when the NC response is free of kinetic effects, and propagated the error to the respective pressure value. The results, shown in Supporting Table 1, indicate that the precision on the pressure values measured through the ratiometric response of the NCs is better than 1% for any pressure between 10–3 and 1 bar. In order to describe the pressure sensing behavior of our DiB NCs in more quantitative terms, in Figure.S5 we report the Langmuir plot of the luminescence pressure response, together with its analysis using a global fit to the multisite Toth's version of the Langmuir model, which accounts for the heterogeneity of the adsorption sites on the NC surfaces. (70) The model adequately reproduces the response of both the core and the shell using the same Langmuir adsorption binding constant K = 46.89 M–1 and the heterogeneity factor m = 0.56. The latter value is significantly different from m = 1 (a characteristic of homogeneous surfaces), which confirms the appropriateness of the Toth's approach.

Interestingly, the strong response to the O2 pressure leads to significant change of the total emission color, as displayed in Figure 3d, which shows the projection of the emission color coordinates extracted from the

PL spectra of Figure 3a onto the Commission Internationale de l'Éclairage (CIE) chromaticity diagram. The color change is easily appreciated by examining the photographs of the DiB NCs film taken at P = 1 bar and P = 10–3 bar under UV illumination (Figure 3e). At atmospheric pressure, the film appears red, due to the dominant contribution of the core emission at 632 nm (see PL spectra in Figure 3a). Upon lowering the O2 pressure to 10–3 bar, the total emission color turns whitish, as a result of the contribution from strong green emission from the CdS shell. Importantly, because the core and shell emissions are fully spectrally separated (Figures 2a and 3a), their respective signals are collected selectively by the red and green detection channels with no cross readout. This is highlighted in the right panels of Figure 3e, showing a strong red signal and essentially no green emission at P = 1 bar. Under vacuum, the green signal increases significantly, while the red channel shows a concomitant dimming, in agreement with the quenching of the core PL observed upon evacuation of the sample chamber (Figure 3a–c).

In order to assess the stability of our r-PSP and the reproducibility of the sensing response, in Figure 4a we report the spectrally integrated intensity of the core and shell emissions during many O2/vacuum cycles in which the PL is continuously monitored while the sample chamber is rapidly evacuated from atmospheric pressure to 10–1, 10–2 and 10–3 bar. Each pressure is maintained for 90 s after which the initial O2 pressure is rapidly restored. For any final vacuum level, the luminescence response of both the core and the shell closely correlates with the pressure change, which is particularly relevant for high frequency sensing measurements. This is a direct consequence of both the ultrafast nature of the electron trapping process and the fact that our r-PSPs can be processed by depositing the DiB NCs directly onto the substrate without the need for a polymeric binder that typically leads to long response times due to slow permeation of molecular oxygen. (55) The initial emission intensity is fully recovered after each cycle, thus confirming the reproducibility of the sensing response and ensuring that the capping ligands are intact.

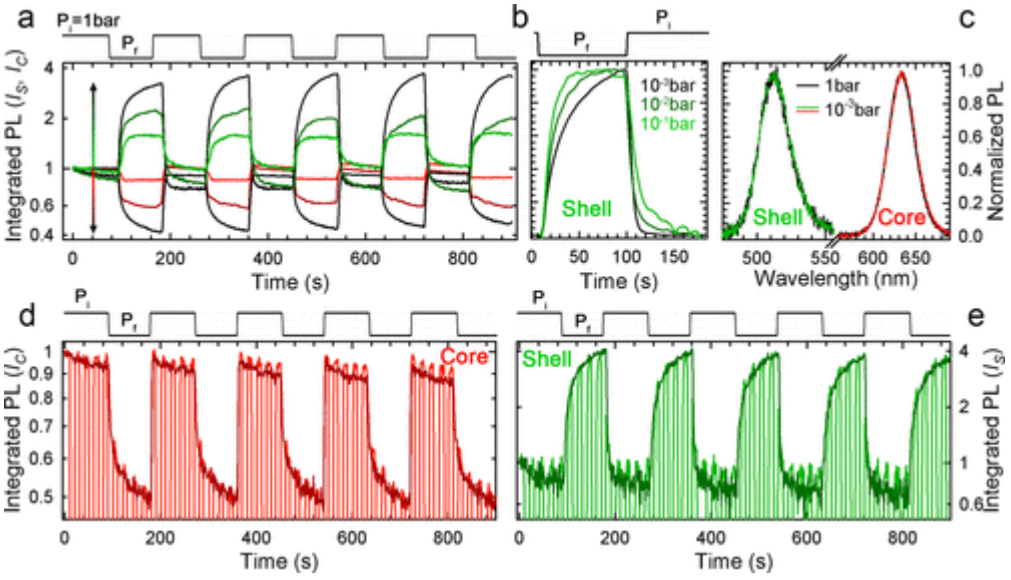

Figure 4. Reproducibility and dynamics of the sensing response. (a) Integrated PL intensity of the NC core (red, brown, and black lines) and the NC shell (light green, dark green, and black lines) during O2/vacuum cycles, starting from atmospheric pressure (Pi = 1 bar) down to different final pressures, Pf = 10–1, 10–2, and 10–3 bar, as indicated by arrows. The pressure steps are shown on the top of the panel for each Pi – Pf step. (b) Evolution of the shell PL extracted from panel a as a function of time for the three O2 pressure ranges, normalized at their maximum value. (c) Normalized shell and core PL spectra at P = 1 bar (solid black lines) and P = 10–3 bar (dashed green and red lines). Integrated PL intensity of (d) core (IC, red line) and (e) shell (IS, green line) during On/Off pressure cycles from atmospheric oxygen pressure (Pi = 1 bar) down to Pf = 10–3 bar collected under continuous (darker lines) or intermittent (lighter lines) illumination.

All measurements are carried out at room temperature using 400 nm excitation; 1 s acquisition time; each pressure step lasts 90 s.

We notice that upon evacuating the sample chamber from 1 bar to 10–1 bar, the PL intensity of both the core and the shell closely follows the O2 pressure change, leading to an approximately 2-fold increase of the shell emission intensity and ∼20% dimming of the core PL, followed by a plateau at a constant pressure. On the other hand, at P = 10–2 to 10–3 bar, the PL brightening/dimming is more pronounced (Figures 3a,b and 4a) and proceeds in time even after the chamber pressure has stabilized. This effect is highlighted in Figure 4b, where we display the shell PL traces of Figure 4a normalized to their intensity maximum for clarity; similar trends are observed for the core emission as illustrated in Figure.S6. These observations point to the coexistence of two interaction regimes between the NCs and O2 that respectively dominate the sensing behavior under high- and low-pressure conditions. The first is responsible for the stepwise PL response concurrent to the removal of ∼99.9% of O2 from the sample chamber and is ascribed to suppressed electron trapping by collisional interaction between the NC film and molecular oxygen. Accordingly, pumping O2 back into the chamber results in essentially instantaneous dimming of the shell PL due to largely increased availability of gaseous O2 molecules in direct contact with the NCs. The second regime leads instead to the slow progressive brightening at lower pressure, which is most likely owing to the gradual desorption of adsorbed O2 molecules that require a larger driving force to detach from the NCs surfaces. Notably, no shift of the core and shell PL peak is observed (Figure 4c), which confirms that the sensing response is not due to permanent oxidation/reduction of the NCs surfaces. (34) In order to further assess the suitability of our r-PSPs for extended time applications, we tested their stability over prolonged exposure to continuous illumination and O2/vacuum cycles. Detailed measurements of the sensing response including extended scans of over 10 consecutive O2/vacuum cycles between 1 and 2 bar O2 pressure with different time intervals, and the stability test under UV illumination for over 2 h are reported in Figures.S7–S11. All measurements show full repeatability and stability over time, with no losses of both the PL intensity and the sensing capability over several hours of continuous sensing.

From the point of view of prospective applications, it is also important to understand whether the interaction between the NCs and molecular O2 is a photoassisted process, as this might affect the accuracy of pressure measurements. To evaluate the effect of exact excitation conditions on the measured radiometric response, we have performed On/Off pressure sensing measurements using the same experimental procedure as the one described above while monitoring the NC emission under either continuous or pulsed (10 s pulse duration) 400 nm excitation. For direct comparison between the two excitation conditions, in Figure 4d,e we report the intensity traces for the core and the shell, respectively, with five cycles collected using pulsed excitation and five cycles monitored under continuous illumination. No differences in the sensing response are observed, which indicates that the NC–O2 interaction occurs identically under “dark” and “light” conditions. A perfect overlap between the PL trends is also found for the core emission excited at 532 nm as reported in Figure.S12.

Single Particle Ratiometric Oxygen Sensing Using DiB NCs

As we show below, an important feature of DiB NCs is that they behave as ratiometric pressure sensors even at the single-NC level, which makes them capable of reporting O2 pressure variations with nanoscale spatial resolution. This represents a unique advantage over PSPs based on chromophores blends and simplifies the paint processing by removing issues associated with the inhomogeneous distribution of the emitters on the model surfaces or in the binder, the factors that typically reduce the spatial accuracy in submicron-scale pressure studies. (60)

The ratiometric sensing ability of individual DiB NCs is demonstrated in Figure 5, where we show confocal imaging and micro-PL data of isolated NCs (drop casted from a diluted hexane solution onto a quartz

substrate with a nominal NC density of ~0.1/µm2) as a function of the O2 pressure. Upon raising the pressure from 10–3 to 1 bar, all NCs show a progressive transition in their emission color from green, to orange, and then red, which is in perfect agreement with the results of the ensemble measurements (Figure 3e). Figure.5b reports the histogram of the IC/IS ratio for 40 individual DiB NCs as a function of the chamber pressure, showing remarkable homogeneity of the ratiometric response across the NC population. This indicates that individual DiB NCs can indeed be used as highly accurate nanoscale ratiometric pressure (or O2) sensors. Importantly, the ratiometric sensing response IC/IS is independent of the total emission intensity, as highlighted in the correlation plot of IC/IS versus (IC + IS) in Figure 5c.

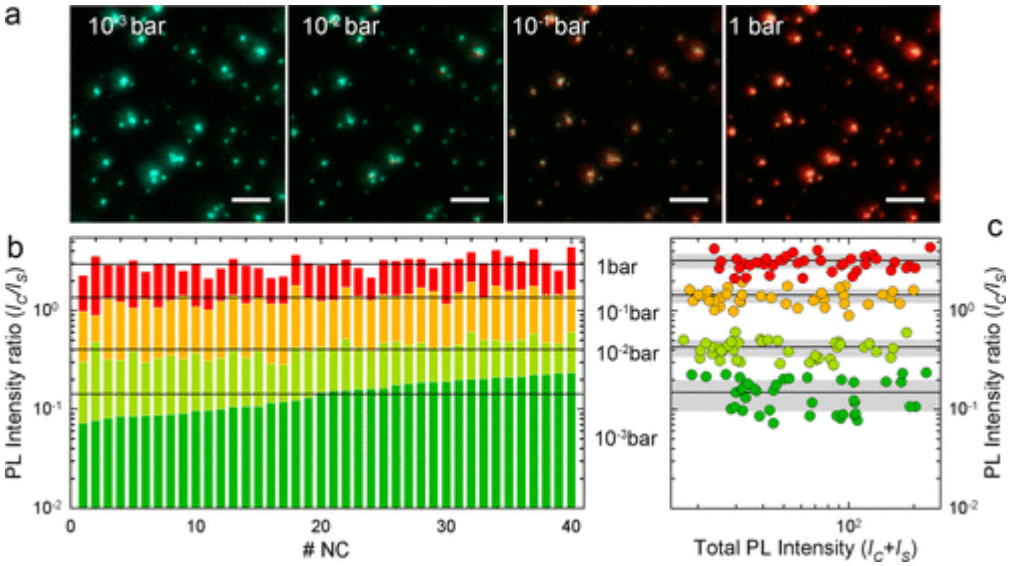

Figure 5. Single particle ratiometric oxygen sensing. (a) A large-area spectrally resolved image of a collection of individual DiB NCs as a function of the O2 pressure under 400 nm excitation (excitation fluence 7 µJ/cm2), showing a progressive change of the emission color from green to red upon increasing the chamber pressure. The scale bar corresponds to 5 µm. (b) Histogram of the single-particle ratiometric response expressed as IC/IS for 40 individual NCs at the monitored oxygen pressures. (c) Correlation plot of the ratiometric sensing response IC/IS versus the total PL intensity (IC + IS) at increasing O2 pressure, indicating that the sensing response is independent of the total emission intensity. The same color code applies to all panels and resembles the total emission color of the NCs: 10–3 bar, dark green; 10–2 bar, light green; 10–1 bar, orange; 1 bar, red. The mean values averaged across the whole NC population are indicated by black solid lines; the respective standard deviations are shown by gray shading.

Photophysical Mechanisms of the Double Sensing Response

In order to gain a deeper insight into the photophysical mechanisms underpinning the ratiometric sensing response of DiB NCs, we have measured the decay dynamics of both the shell and the core luminescence in a controlled atmosphere (Figure 6a,b). We start our analysis with the reversed pressure response of the core luminescence, which is key for the realization of the “double sensing” regime. Examining the core time-resolved PL traces in Figure 6a we note a ~20% increase of the zero-delay PL intensity with decreasing pressure from 1 bar to 10–3 bar, which is accompanied by the acceleration of the decay dynamics. These are the typical spectroscopic signatures of the recombination of charged excitons (trions) consisting of a photoexcited electron–hole pair and a pre-existing carrier (in the case of CdSe/CdS NCs it is predominantly an electron (51, 71, 72)) produced by photoionization. (63, 67) In atmospheric conditions (Figure 6c), molecular oxygen continuously removes excess electrons thereby hindering the formation of negative trions. As a result, the spectroscopic behavior of the DiB NCs is dominated by neutral excitons. If these excitons are core-localized, they are virtually unaffected by surface species due to the protective effect of

the ultrathick CdS shell. Upon evacuation, the oxygen-driven “discharging” process is gradually suppressed, resulting in the formation of negative trions. These species are characterized by an increased emission rate (it is ideally twice that of a neutral exciton), which can explain the increase in the early time PL amplitude observed upon reducing the amount of oxygen in the sample chamber.

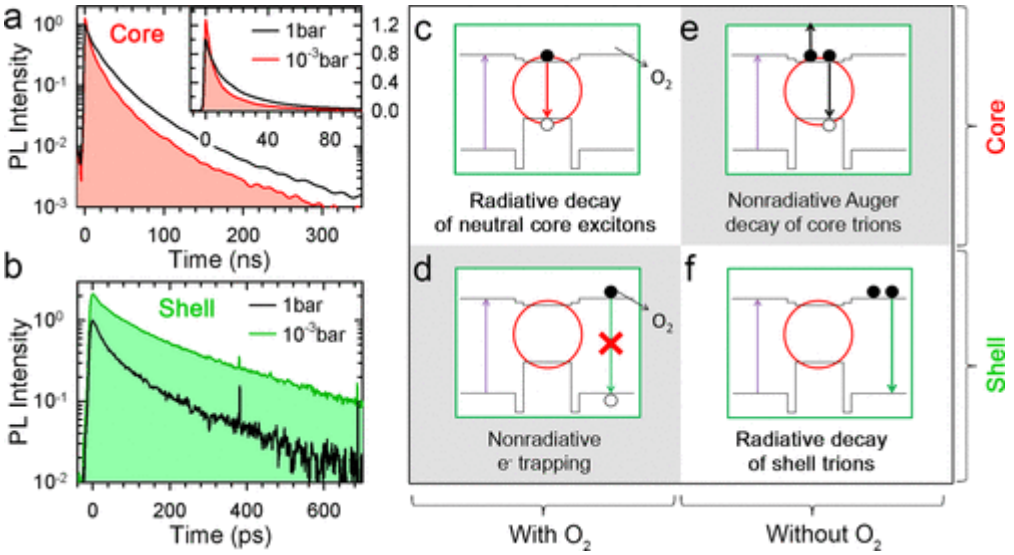

Figure 6. Photophysical mechanism of the dual sensing response. PL decay curves of (a) core and (b) shell emission measured at P = 1 bar (red and green lines, respectively) and P = 10–3 bar (black lines). The inset in panel a reports the decay curve of the core PL using a linear scale to highlight the increase in the intensity at zero delay time as well as the accelerated decay exhibited at low O2 pressures. Schematics of the NC-O2 interaction leading to the observed optical responses: In the presence of O2, (c) neutral core excitons recombine radiatively, while (d) the shell-exciton decay is affected by nonradiative electron processes involving either direct electron extraction by O2 molecules or trapping at surface defects depleted of electrons due to interactions with O2. In the absence of O2, enhanced availability of excess electrons makes nonradiative Auger decay the dominant recombination pathway for negatively charged core excitons (e), while shell excitons decay radiatively thanks to impeded electron capture by O2 and suppressed Auger recombination (f); the latter is diminished due to a large volume of the shell. The regimes dominated by nonradiative recombination are highlighted by gray shading.

In addition, we observe the reduction of the PL lifetime, which is due to a combined effect of the enhanced radiative decay and the activation of nonradiative Auger recombination. In DiB NCs with a sharp core/shell interface, the Auger process is not as strongly suppressed as in graded or interfacially alloyed thick-shell CdSe/CdS NCs that could exhibit nearly unity trion PL quantum yields. (73, 74) As a result, the dominant decay channel for the core PL in the absence of O2 is nonradiative Auger recombination of negatively charged excitons (Figure 6d).

The formation of negative trions in NC samples under vacuum is confirmed by circular polarization-resolved PL measurements in high magnetic fields reported in Figure.S13. This data shows that, similarly to giant core/shell CdSe/CdS nanocrystals and core/shell CdSe/CdSe nanoplatelets, magneto-PL from DiB NCs exhibits circular polarization typical of negatively charged excitons. (67, 75) We note that O2/vacuum scans using core-selective excitation at 532 nm reported in Figure.S12 show similar dimming of the core PL as that observed using 400 nm excitation, thereby unambiguously confirming that the sensitivity of core emission to O2 is due only to nonradiative Auger recombination of core trions and not the depletion of the NC conduction band due to progressively more efficient shell emission observed for decreasing O2 pressure.

Next, we investigate the effect of O2 on the shell-PL dynamics. Because the thickness of the CdS shell (8.5 nm) is greater than the exciton Bohr radius in CdS (5.6 nm), the shell excitons are bulklike and hence are virtually unaffected by Auger recombination. The rate of Auger decay scales inversely with the particle volume and, therefore, is expected to be over 300 times lower than in the 1.5 nm CdSe core. (76) As a result, even in the case of excess electrons, as indicated by circular polarization-resolved magneto-PL measurements in Figure.S13, the nonradiative decay of shell excitons is primarily not due to Auger recombination, but still surface trapping (Figure 6e). Accordingly, lowering the chamber pressure, which is equivalent to raising the Fermi levels, leads to passivation of electron surface traps, which is manifested in the strong increase of the zero delay PL intensity, accompanied by the extension of the PL lifetime (Figure 6b,f). The resulting effect of these changes is the >300% enhancement of the emission intensity observed in cw measurements (Figure 3b). This confirms that the shell PL dynamics is dominated by activation/suppression of electron capture either directly by O2 or electron-deficient surface traps. This further points to the coexistence of two trapping processes occurring on two different time scales: (i) ultrafast electron capture with the characteristic time unresolvable in our measurements with ∼6 ps resolution (streak-camera detection), thereby modulating the zero-delay PL intensity without affecting its temporal dynamics, and (ii) a slower electron trapping channel competing with radiative recombination of shell excitons, whose progressive suppression at decreasing pressure leads to slower PL dynamics. (36, 77) Further evidence of the dominant effect of oxygen on the PL intensity of core and shell excitons is provided by On/Off pressure cycling with other gases, as reported in Figures.S14 and S15. Specifically, the PL intensity of both the core and the shell was recorded while filling the sample chamber with CO2 (Figure.S14) and humid air (Figure.S15). The ratiometric double sensing response is also observed upon exposure of the NCs to CO2, although with a weaker sensitivity than in the case of oxygen due to a weaker reactivity of CO2. This observation suggests that DiB NCs can also be applied as environmental gas sensors. Furthermore, data indicate (Figure.S15) that the sensing response to wet air is similar to that observed for dry O2, which suggests that humidity has a negligible effect on the PSP behavior. This extends the potential use of DiB NCs as gas flow sensors in ambient conditions without distortions due to variations in humidity.

Beside their implications in pressure sensing, the conducted studies reveal an important fundamental connection between the effect of changing oxygen pressure outside the NC and the NC Fermi level, which is largely analogous to the effect of the applied potential in electrochemical experiments. (66) Specifically, as shown in Figure.S16, the application of a negative potential to DiB-NCs leads to the gradual increase of the shell emission and the concomitant dimming of the core PL. At V = −1 V, the core PL dynamics shows typical signatures of trion decay, indicating direct injection of electrons into the NC conduction band states. The value of this injection potential is consistent with expectations for undoped NCs with Eg = 1.9 eV (the core band gap) wherein the Fermi level is near the center of the energy gap. This further confirms that the potential drop outside the NCs in the spectro-electrochemical measurements is essentially negligible leading to one-to-one correspondence between the applied potential and the position of the Fermi level.

The effect of reduced oxygen pressure on the NC's emission intensity and dynamics (Figures 3b and 6a,b) shows a striking similarity to that of the electrochemical potential (Figure.S17). Specifically, progressive removal of oxygen from the NC surrounding area leads to the rise of the Fermi level such that eventually it can reach the position of the conduction band (at ∼10–3 bar). At this point, excess electrons are injected into the NC quantized states leading to formation of negative core trions under optical excitation (Figure.S13). A similar behavior has been previously observed for CdSe/CdS nanoplatelets. (36) Notably, the magneto-optical data for DiB-NCs shown in Figure.S13 further indicate that the effect of charging with extra electrons is not limited to core states but also affects shell states, resulting in formation of negative shell-based trions. The effect of the Fermi energy modulation on the dual-color emission of DiB NCs was modeled in ref 63 as a function of occupancy of surface states, which allowed for closely describing the observed behaviors for both the core and the shell PL.

We note that the regime of hole injection can also, in principle, be realized by applying sufficiently large positive electrochemical potentials or, in direct analogy, exposing the NCs to high oxygen pressure. However, because the valence band energy of the CdS shell is ∼1.5 eV below the intrinsic-NC Fermi level, strongly oxidative conditions required for hole injection usually result in significant NC damage accompanied by PL quenching. As discussed, for example, in ref 63, the PL quantum yield does not fully recover after NCs are exposed to about +1 V oxidative potential, which is indicative of their photochemical degradation.

In conclusion, we have demonstrated the first example of a ratiometric O2-sensing PSP based on a single type of two-color emitter, which features (i) intrinsic ratiometric response at the single particle level, (ii) negligible overlap between the luminescence spectra of the reference and the sensor, (iii) enhanced sensitivity to O2 partial pressure, and (iv) temperature-independent ratiometric behavior. Because of the shell- and core-PL bands of the DiB NCs exhibit trends of opposite directions in response to exposure to oxygen, our "double-sensor" r-PSPs demonstrate an enhanced pressure sensitivity with respect to that achievable with traditional reference-sensor pairs, where the reference channel is "neutral," that is, not sensitive to O2. Specifically, as a result of the direct exposure of shell excitons to the NC surfaces, the shell luminescence is strongly affected by electron withdrawing by O2, which leads to progressive emission quenching with increasing oxygen pressure. In direct contrast, the core PL is enhanced in the presence of oxygen that helps maintain NCs in the neutral state by removing extra electrons that otherwise trigger fast nonradiative Auger recombination. As a result of these opposing trends, the ratiometric response of the NCs is largely amplified with respect to that achievable by monitoring the individual emissions of the core and the shell. Temperature-controlled PL measurements reveal that temperature-induced changes in pressure sensitivity are negligibly small in the interval between 0 and 70 °C. The sensing response probed both at the ensemble and at the single-particle level using continuous and pulsed excitation is fully reproducible and unaffected by prolonged UV illumination. Finally, a nearly complete spectral separation between the core and the shell emission bands leads to no cross-readout between the two detection channels.

Methods

Synthesis of DiB NCs

DiB NCs NCs were synthesized following the procedure described in ref 49. Briefly, zincblende CdSe NCs were synthesized by previously reported methods. (78) For the synthesis of CdSe (R0 = 1.5 nm)/CdS NCs, 2 × 10–7 mol of CdSe NCs (purified twice) dispersed in 10 mL of 1-octadecene (ODE) were loaded into a 100 mL flask, degassed at 110 °C for 1 h. The flask was filled with Ar, and heated up to 300 °C for CdS shell growth. A 0.2 mmol sample of Cd-oleate and 0.2 mmol of 1-dodecanethiol were added slowly (0.1 mmol/min) and the reaction was maintained at the elevated temperature for 30 min to form a thin CdS buffer layer (∼3 monolayers) on top of the CdSe cores. For further CdS shell growth, a mixed solution of Cd-oleate and trioctylphospine-sulfur (0.5 M/0.5 M) in ODE was continuously added at a rate of 1 mmol/hour at 300 °C. After the injection of precursors was completed, the reaction products were cooled to room temperature and purified repeatedly by a precipitation-and-redispersion method. The final products were dispersed in hexane for further characterization.

Spectroscopic Studies

Optical absorption and emission measurements were performed on thin films dip-casted on quartz substrates. Optical absorption spectra were measured with a Varian Cary 50 spectrophotometer. Steady-state and time-resolved photoluminescence (PL) spectra were excited by a frequency-doubled Ti:sapphire laser (400 nm, pulse duration 150 fs, repetition rate 76 MHz). PL spectra were collected with a liquid-nitrogen-cooled Instrument SA Spectrum One charge-coupled device (CCD) coupled to a Horiba Scientific Triax 180 monochromator. The PL dynamics of shell emission in the subnanosecond time regime were

measured with a Hamamatsu streak camera. The PL dynamics of core emission in the nanosecond time regime were studied with the same Ti:sapphire laser as an excitation source but reducing its repetition rate to 760 kHz with a pulse picker based on a Conoptics 350-160 electro-optical modulator. The PL dynamics were measured with a Hamamatsu R943-02 time-correlated single-photon counting unit coupled to an Oriel Instruments Cornerstone 260 monochromator.

For magneto-optical measurements, the samples were mounted in the variable temperature insert of a split-coil cryo-magnet with direct optical access. The PL was excited with the same frequency-doubled Ti:sapphire laser and the circularly polarized emission was selected using a quarter-wave plate coupled with a linear polarizer. The signal was monitored using a CCD camera coupled to a 6 m long optical fiber to ensure full depolarization of the emitted light.

Pressure Sensing Experiments

For oxygen pressure studies, a few monolayer films of DiB NCs were deposited onto quartz substrates by dip-casting from diluted hexane solutions (optical density of 0.05 at 500 nm; 2 dips for 10 s). The films were successively mounted in a sealed chamber with direct optical access and the PL was monitored using the setup described above both as a function of the oxygen pressure and during O2/vacuum cycles to test the reversibility of the quenching process. Before any pressure ramp, the PL efficiency has been preliminary monitored for several minutes in O2 in order to evaluate possible photobrightening effects due to UV curing of surface defects. No photobrightening has been observed for any of the investigated samples. The same procedure has been followed for PL-sensing measurements using CO2 (purity grade 4.5, ≥99.995 vol %) and humid air (20.5 g kg–1).

For single particle PL sensing experiments, the DiB NCs were deposited onto a glass substrate from a very diluted hexane solution and loaded into an Oxford Instrument Microscopy Cryostat. Confocal imaging was performed using a Nikon Ti-U inverted microscope and exciting the NCs with a frequency-doubled Ti:sapphire laser (400 nm, 7 μJ/cm2). In collecting single particle data, large NC aggregates were excluded from the statistics. Photographs of the NC film and isolated particles in O2 and vacuum conditions were taken using a Canon EOS 400D camera.

The Supporting Information is available free of charge on the ACS Publications website at DOI: 10.1021/acs.nanolett.6b04577.

Author Information

ARTICLE SECTIONSJump To

Corresponding Authors

Victor I. Klimov - Chemistry Division and Center for Advanced Solar Photophysics, Los Alamos National Laboratory, Los Alamos, New Mexico 87545, United States; Orcidhttp://orcid.org/0000-0003-1158-3179; Email: klimov@lanl.gov

Sergio Brovelli - Dipartimento di Scienza dei Materiali, Università degli Studi di Milano-Bicocca, via Cozzi 55, I 20125 Milano, Italy; Orcidhttp://orcid.org/0000-0002-5993-855X; Email: sergio.brovelli@unimib.it

Authors

Monica Lorenzon - Dipartimento di Scienza dei Materiali, Università degli Studi di Milano-Bicocca, via Cozzi 55, I 20125 Milano, Italy; Orcidhttp://orcid.org/0000-0003-3524-9546

Valerio Pinchetti - Dipartimento di Scienza dei Materiali, Università degli Studi di Milano-Bicocca, via Cozzi 55, I 20125 Milano, Italy

Francesco Bruni - Dipartimento di Scienza dei Materiali, Università degli Studi di Milano-Bicocca, via Cozzi 55, I 20125 Milano, Italy

Wan Ki Bae - Chemistry Division and Center for Advanced Solar Photophysics, Los Alamos National Laboratory, Los Alamos, New Mexico 87545, United States; Orcidhttp://orcid.org/0000-0002-3832-2449

Francesco Meinardi - Dipartimento di Scienza dei Materiali, Università degli Studi di Milano-Bicocca, via Cozzi 55, I 20125 Milano, Italy

Notes

The authors declare no competing financial interest.

Acknowledgment

Financial support from Fondazione Cariplo is acknowledged by S.B. and F.M. through Grant 2012-0844. M.L. thanks the Fondazione Cassa di Risparmio di Tortona for support. V.I.K. and W.K.B. were supported by the Chemical Sciences, Biosciences, and Geosciences Division, Office of Basic Energy Sciences, Office of Science, U.S. Department of Energy. S.B. wishes to thank the European Community's Seventh Framework Programme (FP7/2007-2013) under Grant Agreement 324603 for financial support (EDONHIST).

References

1Liu, T.; Sullivan, J. Pressure and temperature sensitive paints; Springer: Berlin, 2005.Google Scholar

2Wolfbeis, O. S. Adv. Mater. 2008, 20, 3759– 3763 DOI: 10.1002/adma.200702276 [Crossref], Google Scholar

3Disotell, K.; Peng, D.; Juliano, T.; Gregory, J.; Crafton, J.; Komerath, N. Exp. Fluids 2014, 55, 1– 15 DOI: 10.1007/s00348-014-1671-2 [Crossref], [CAS], Google Scholar

4Gregory, J. W.; Sakaue, H.; Liu, T.; Sullivan, J. P. Annu. Rev. Fluid Mech. 2014, 46, 303– 330 DOI: 10.1146/annurev-fluid-010313-141304 [Crossref], Google Scholar

5Gregory, J. W.; Sullivan, J. P.; Raman, G.; Raghu, S. AIAA J. 2007, 45, 568– 576 DOI: 10.2514/1.26127 [Crossref], Google Scholar

6Nagai, H.; Naraoka, R.; Sawada, K.; Asai, K. AIAA J. 2008, 46, 215– 222 DOI: 10.2514/1.28371 [Crossref], [CAS], Google Scholar

7Niimi, T.; Yoshida, M.; Kondo, M.; Oshima, Y.; Mori, H.; Egami, Y.; Asai, K.; Nishide, H. J. Thermophys. Heat Transfer 2005, 19, 9– 16 DOI: 10.2514/1.5047 [Crossref], [CAS], Google Scholar

8Gregory, J.; Sullivan, J.; Sakaue, H.; Huang, C. Y. Molecular sensors for MEMS. In 40th AIAA Aerospace Sciences Meeting & Exhibit; American Institute of Aeronautics and Astronautics: Washington, DC, 2002.[Crossref], Google Scholar

9Dickert, F. L.; Besenböck, H.; Tortschanoff, M. Adv. Mater. 1998, 10, 149– 151 DOI: 10.1002/(SICI)1521-4095(199801)10:2<149::AID-ADMA149>3.0.CO;2-2 [Crossref], Google Scholar

10Frederiksen, M. S.; Glud, R. N. Limnol. Oceanogr. 2006, 51, 1072– 1083 DOI: 10.4319/lo.2006.51.2.1072 [Crossref], Google Scholar

11Sánchez-Barragán, I.; Costa-Fernández, J. M.; Sanz-Medel, A.; Valledor, M.; Campo, J. C. TrAC, Trends Anal. Chem. 2006, 25, 958– 967 DOI: 10.1016/j.trac.2006.07.009 [Crossref], Google Scholar

12Babilas, P.; Liebsch, G.; Schacht, V.; Klimant, I.; Wolfbeis, O. S.; Szeimies, R.-M.; Abels, C. Microcirculation 2005, 12, 477– 487 DOI: 10.1080/10739680591003314 [Crossref], Google Scholar

13Wu, M.; Lin, Z.; Schäferling, M.; Dürkop, A.; Wolfbeis, O. S. Anal. Biochem. 2005, 340, 66– 73 DOI: 10.1016/j.ab.2005.01.050 [Crossref], Google Scholar

14Amao, Y.; Ishikawa, Y.; Okura, I. Anal. Chim. Acta 2001, 445, 177– 182 DOI: 10.1016/S0003-2670(01)01254-5 [Crossref], Google Scholar

15Sakaue, H.; Miyamoto, K.; Miyazaki, T. J. Appl. Phys. 2013, 113, 084901 DOI: 10.1063/1.4792761 [Crossref], Google Scholar

16Wang, X.-d.; Wolfbeis, O. S. Chem. Soc. Rev. 2014, 43, 3666– 3761 DOI: 10.1039/C4CS00039K [Crossref], [PubMed], [CAS], Google Scholar

17Papkovsky, D. B.; Dmitriev, R. I. Chem. Soc. Rev. 2013, 42, 8700– 32 DOI: 10.1039/c3cs60131e [Crossref], Google Scholar

18Schaferling, M. Angew. Chem., Int. Ed. 2012, 51, 3532– 54 DOI: 10.1002/anie.201105459 [Crossref], Google Scholar

19Mosser, V.; Suski, J.; Goss, J.; Obermeier, E. Sens. Actuators, A 1991, 28, 113– 132 DOI: 10.1016/0924-4247(91)85020-O [Crossref], Google Scholar

20Li, M.; Wang, M.; Li, H. Opt. Express 2006, 14, 1497– 1504 DOI: 10.1364/OE.14.001497 [Crossref], Google Scholar

21Bell, J. H.; Schairer, E. T.; Hand, L. A.; Mehta, R. D. Annu. Rev. Fluid Mech. 2001, 33, 155– 206 DOI: 10.1146/annurev.fluid.33.1.155 [Crossref], Google Scholar

22Khalil, G. E.; Costin, C.; Crafton, J.; Jones, G.; Grenoble, S.; Gouterman, M.; Callis, J. B.; Dalton, L. R. Sens. Actuators, B 2004, 97, 13– 21 DOI: 10.1016/S0925-4005(03)00484-2 [Crossref], [CAS], Google Scholar

23Amao, Y.; Miyashita, T.; Okura, I. React. Funct. Polym. 2001, 47, 49– 54 DOI: 10.1016/S1381-5148(00)00070-5 [Crossref], [CAS], Google Scholar

24Basu, B. J.; Anandan, C.; Rajam, K. S. Sens. Actuators, B 2003, 94, 257– 266 DOI: 10.1016/S0925-4005(03)00450-7 [Crossref], [CAS], Google Scholar

25Demas, J. N.; DeGraff, B. A., Design and Applications of Highly Luminescent Transition Metal Complexes. In Topics in Fluorescence Spectroscopy; Lakowicz, J. R., Ed.; Springer: New York, 1994; Vol. 4, pp 71–107.Google Scholar

26Liu, T.; Guille, M.; Sullivan, J. P. AIAA J. 2001, 39, 103– 112 DOI: 10.2514/3.14703 [Crossref], Google Scholar

27Yasuhiro, E.; Keisuke, A., Effects of Antioxidants on Photodegradation of Porous Pressure-Sensitive Paint. In 22nd AIAA Aerodynamic Measurement Technology and Ground Testing Conference, American Institute of Aeronautics and Astronautics: Washington, DC, 2002.Google Scholar

28Gregory, J. W.; Asai, K.; Kameda, M.; Liu, T.; Sullivan, J. P. Proc. Inst. Mech. Eng., Part G 2008, 222, 249–290 DOI: 10.1243/09544100JAERO243 [Crossref], [PubMed], [CAS], Google Scholar

29Bell, J. H. Accuracy limitations of lifetime-based pressure-sensitive paint (PSP) measurements; Instrumentation in Aerospace Simulation Facilities, 2001. 19th International Congress on ICIASF 2001, Aug. 27–30, 2001, IEEE: Piscataway, NJ, 2001; pp 5– 16.Google Scholar

30Borisov, S. M.; Vasylevska, A. S.; Krause, C.; Wolfbeis, O. S. Adv. Funct. Mater. 2006, 16, 1536– 1542 DOI: 10.1002/adfm.200500778 [Crossref], Google Scholar

31Stich, M. I. J.; Nagl, S.; Wolfbeis, O. S.; Henne, U.; Schaeferling, M. Adv. Funct. Mater. 2008, 18, 1399–1406 DOI: 10.1002/adfm.200701199 [Crossref], Google Scholar

32Köse, M. E.; Omar, A.; Virgin, C. A.; Carroll, B. F.; Schanze, K. S. Langmuir 2005, 21, 9110– 9120 DOI: 10.1021/la050999+ [ACS Full Text ACS Full Text], Google Scholar

33Amelia, M.; Lavie-Cambot, A.; McClenaghan, N. D.; Credi, A. Chem. Commun. 2011, 47, 325– 327 DOI: 10.1039/C0CC02163F [Crossref], Google Scholar

34Cordero, S. R.; Carson, P. J.; Estabrook, R. A.; Strouse, G. F.; Buratto, S. K. J. Phys. Chem. B 2000, 104, 12137– 12142 DOI: 10.1021/jp001771s [ACS Full Text ACS Full Text], Google Scholar

35Liu, Z.; Ma, Q.; Wang, X.; Lin, Z.; Zhang, H.; Liu, L.; Su, X. Biosens. Bioelectron. 2014, 54, 617– 622 DOI: 10.1016/j.bios.2013.11.050 [Crossref], [PubMed], [CAS], Google Scholar

36Lorenzon, M.; Christodoulou, S.; Vaccaro, G.; Pedrini, J.; Meinardi, F.; Moreels, I.; Brovelli, S. Nat. Commun. 2015, 6, 6434 DOI: 10.1038/ncomms7434 [Crossref], [PubMed], [CAS], Google Scholar

37Müller, J.; Lupton, J. M.; Rogach, A. L.; Feldmann, J.; Talapin, D. V.; Weller, H. Appl. Phys. Lett. 2004, 85, 381– 383 DOI: 10.1063/1.1769585 [Crossref], [CAS], Google Scholar

38Nazzal, A. Y.; Qu, L.; Peng, X.; Xiao, M. Nano Lett. 2003, 3, 819– 822 DOI: 10.1021/nl0340935 [ACS Full Text ACS Full Text], [CAS], Google Scholar

39Lau, P. C.; Norwood, R. A.; Mansuripur, M.; Peyghambarian, N. Nanotechnology 2013, 24, 015501 DOI: 10.1088/0957-4484/24/1/015501 [Crossref], Google Scholar

40Xia, Y.; Zhang, T.; Diao, X.; Zhu, C. Chem. Lett. 2007, 36, 242– 243 DOI: 10.1246/cl.2007.242 [Crossref], Google Scholar

41Collier, B. B.; Singh, S.; McShane, M. Analyst 2011, 136, 962– 967 DOI: 10.1039/C0AN00661K [Crossref], Google Scholar

42García-Santamaría, F.; Chen, Y.; Vela, J.; Schaller, R. D.; Hollingsworth, J. A.; Klimov, V. I. Nano Lett. 2009, 9, 3482– 3488 DOI: 10.1021/nl901681d [ACS Full Text ACS Full Text], Google Scholar

43Klimov, V. I.; Mikhailovsky, A. A.; Xu, S.; Malko, A.; Hollingsworth, J. A.; Leatherdale, C. A.; Eisler, H.-J.; Bawendi, M. G. Science 2000, 290, 314– 317 DOI: 10.1126/science.290.5490.314 [Crossref], Google Scholar

44Pal, B. N.; Ghosh, Y.; Brovelli, S.; Laocharoensuk, R.; Klimov, V. I.; Hollingsworth, J. A.; Htoon, H. Nano Lett. 2012, 12, 331– 336 DOI: 10.1021/nl203620f [ACS Full Text ACS Full Text], [CAS], Google Scholar

45Shirasaki, Y.; Supran, G. J.; Bawendi, M. G.; Bulovic, V. Nat. Photonics 2012, 7, 13– 23 DOI: 10.1038/nphoton.2012.328 [Crossref], Google Scholar

46Bae, W. K.; Brovelli, S.; Klimov, V. I. MRS Bull. 2013, 38, 721– 730 DOI: 10.1557/mrs.2013.182 [Crossref], Google Scholar

47Ho, Y.-P.; Leong, K. W. Nanoscale 2010, 2, 60– 68 DOI: 10.1039/B9NR00178F [Crossref], Google Scholar

48Feng, Y.; Cheng, J.; Zhou, L.; Zhou, X.; Xiang, H. Analyst 2012, 137, 4885– 4901 DOI: 10.1039/c2an35907c [Crossref], [PubMed], [CAS], Google Scholar

49Brovelli, S.; Bae, W. K.; Galland, C.; Giovanella, U.; Meinardi, F.; Klimov, V. I. Nano Lett. 2014, 14, 486– 494 DOI: 10.1021/nl403478s [ACS Full Text ACS Full Text], Google Scholar

50Brovelli, S.; Galland, C.; Viswanatha, R.; Klimov, V. I. Nano Lett. 2012, 12, 4372– 4379 DOI: 10.1021/nl302182u [ACS Full Text ACS Full Text], [CAS], Google Scholar

51Galland, C.; Ghosh, Y.; Steinbruck, A.; Sykora, M.; Hollingsworth, J. A.; Klimov, V. I.; Htoon, H. Nature 2011, 479, 203– 207 DOI: 10.1038/nature10569 [Crossref], [PubMed], [CAS], Google Scholar

52Klimov, V. I. Nanocrystal quantum dots; CRC Press: Boca Raton, FL, 2010.[Crossref], Google Scholar

53Pechstedt, K.; Whittle, T.; Baumberg, J.; Melvin, T. J. Phys. Chem. C 2010, 114, 12069– 12077 DOI: 10.1021/jp100415k [ACS Full Text ACS Full Text], Google Scholar

54Ma, J.; Chen, J. Y.; Guo, J.; Wang, C. C.; Yang, W. L.; Xu, L.; Wang, P. N. Nanotechnology 2006, 17, 2083 DOI: 10.1088/0957-4484/17/9/002 [Crossref], Google Scholar

55Kameda, M.; Seki, H.; Makoshi, T.; Amao, Y.; Nakakita, K. Sens. Actuators, B 2012, 171–172, 343– 349 DOI: 10.1016/j.snb.2012.04.049 [Crossref], [CAS], Google Scholar

56Gouterman, M. J. Chem. Educ. 1997, 74, 697 DOI: 10.1021/ed074p697 [ACS Full Text ACS Full Text], Google Scholar

57Xiang, H.; Zhou, L.; Feng, Y.; Cheng, J.; Wu, D.; Zhou, X. Inorg. Chem. 2012, 51, 5208– 5212 DOI: 10.1021/ic300040n [ACS Full Text ACS Full Text], Google Scholar

58Park, J.; Lee, J.; Kwag, J.; Baek, Y.; Kim, B.; Yoon, C. J.; Bok, S.; Cho, S.-H.; Kim, K. H.; Ahn, G. O.; Kim, S. ACS Nano 2015, 9, 6511 DOI: 10.1021/acsnano.5b02357 [ACS Full Text ACS Full Text], Google Scholar

59Borisov, S. M.; Klimant, I. Anal. Chim. Acta 2013, 787, 219– 225 DOI: 10.1016/j.aca.2013.05.032 [Crossref], Google Scholar

60Baleizão, C.; Nagl, S.; Schäferling, M.; Berberan-Santos, M. N.; Wolfbeis, O. S. Anal. Chem. 2008, 80, 6449– 6457 DOI: 10.1021/ac801034p [ACS Full Text ACS Full Text], Google Scholar

61Galland, C.; Brovelli, S.; Bae, W. K.; Padilha, L. A.; Meinardi, F.; Klimov, V. I. Nano Lett. 2013, 13, 321– 328 DOI: 10.1021/nl3045316 [ACS Full Text ACS Full Text], Google Scholar

62Pinchetti, V.; Meinardi, F.; Camellini, A.; Sirigu, G.; Christodoulou, S.; Bae, W. K.; De Donato, F.; Manna, L.; Zavelani-Rossi, M.; Moreels, I.; Klimov, V. I.; Brovelli, S. ACS Nano 2016, 10, 6877– 6887 DOI: 10.1021/acsnano.6b02635 [ACS Full Text ACS Full Text], Google Scholar

63Brovelli, S.; Bae, W. K.; Meinardi, F.; Santiago González, B.; Lorenzon, M.; Galland, C.; Klimov, V. I. Nano Lett. 2014, 14, 3855– 3863 DOI: 10.1021/nl501026r [ACS Full Text ACS Full Text], Google Scholar

64Mosconi, E.; Salvatori, P.; Saba, M. I.; Mattoni, A.; Bellani, S.; Bruni, F.; Gonzalez, B. S.; Antognazza, M. R.; Brovelli, S.; Lanzani, G.; Li, H.; Brédas, J.-L.; Angeli, F. D. ACS Energy Lett. 2016, 1, 454– 463 DOI: 10.1021/acsenergylett.6b00197 [ACS Full Text ACS Full Text], [CAS], Google Scholar

65Bruni, F.; Pedrini, J.; Bossio, C.; Santiago-Gonzalez, B.; Meinardi, F.; Bae, W. K.; Klimov, V. I.; Lanzani, G.; Brovelli, S. Adv. Funct. Mat. DOI: DOI: 10.1002/adfm.201605533 .[Crossref], Google Scholar

66Choi, J.-H.; Oh, S. J.; Lai, Y.; Kim, D. K.; Zhao, T.; Fafarman, A. T.; Diroll, B. T.; Murray, C. B.; Kagan, C. R. ACS Nano 2013, 7, 8275– 8283 DOI: 10.1021/nn403752d [ACS Full Text ACS Full Text], [CAS], Google Scholar

67Javaux, C.; Mahler, B.; Dubertret, B.; Shabaev, A.; Rodina, A. V.; Efros, Al. L.; Yakovlev, D. R.; Liu, F.; Bayer, M.; Camps, G.; Biadala, L.; Buil, S.; Quelin, X.; Hermier, J. P. Nat. Nanotechnol. 2013, 8, 206– 212 DOI: 10.1038/nnano.2012.260 [Crossref], [PubMed], [CAS], Google Scholar

68Liu, F.; Biadala, L.; Rodina, A. V.; Yakovlev, D. R.; Dunker, D.; Javaux, C.; Hermier, J.-P.; Efros, A. L.; Dubertret, B.; Bayer, M. Phys. Rev. B: Condens. Matter Mater. Phys. 2013, 88, 035302 DOI: 10.1103/PhysRevB.88.035302 [Crossref], [CAS], Google Scholar

69ISSI - Pressure Sensitive Paints. http://www.psp-tsp.com/index.php?id=115. (Accessed Dec 30, 2016).Google Scholar

70Toth, J. Acta Chim Acad. Sci. Hungar 1971, 69, 311– 328[CAS], Google Scholar

71Javaux, C.; Mahler, B.; Dubertret, B.; Shabaev, A.; Rodina, A. V.; Efros, A. L.; Yakovlev, D. R.; Liu, F.; Bayer, M.; Camps, G.; Biadala, L.; Buil, S.; Quelin, X.; Hermier, J. P. Nat. Nanotechnol. 2013, 8, 206– 212 DOI: 10.1038/nnano.2012.260 [Crossref], [PubMed], [CAS], Google Scholar

72Jha, P. P.; Guyot-Sionnest, P. ACS Nano 2009, 3, 1011– 1015 DOI: 10.1021/nn9001177 [ACS Full Text ACS Full Text], Google Scholar

73Park, Y. S.; Malko, A. V.; Vela, J.; Chen, Y.; Ghosh, Y.; García-Santamaría, F.; Hollingsworth, J. A.; Klimov, V. I.; Htoon, H. Phys. Rev. Lett. 2011, 106, 187401 DOI: 10.1103/PhysRevLett.106.187401 [Crossref], Google Scholar

74Nasilowski, M.; Spinicelli, P.; Patriarche, G.; Dubertret, B. Nano Lett. 2015, 15, 3953 DOI: 10.1021/acs.nanolett.5b00838 [ACS Full Text ACS Full Text], Google Scholar

75Christodoulou, S.; Vaccaro, G.; Pinchetti, V.; De Donato, F.; Grim, J. Q.; Casu, A.; Genovese, A.; Vicidomini, G.; Diaspro, A.; Brovelli, S.; Manna, L.; Moreels, I. J. Mater. Chem. C 2014, 2, 3439– 3447 DOI: 10.1039/c4tc00280f [Crossref], [CAS], Google Scholar

76Robel, I.; Gresback, R.; Kortshagen, U.; Schaller, R. D.; Klimov, V. I. Phys. Rev. Lett. 2009, 102, 177404 DOI: 10.1103/PhysRevLett.102.177404 [Crossref], [PubMed], [CAS], Google Scholar

77Lakowicz, J. Principles of Fluorescence Spectroscopy, 3rd ed.; Springer: New York, 2006.[Crossref], Google Scholar

78Yang, Y. A.; Wu, H.; Williams, K. R.; Cao, Y. C. Angew. Chem., Int. Ed. 2005, 44, 6712– 6715 DOI: 10.1002/anie.200502279 [Crossref], Google Scholar